Applied Physics Laboratory
University of Washington

1013 NE 40th Street
Box 355640
Seattle, WA 98105-6698

206-543-1300
FAX 206-543-6785
www.apl.washington.edu

10 April 2020

To: Dr. Raymond J. Soukup
Office of Naval Research (Code 322)
875 North Randolph Street
Arlington, VA 22203-1995

From: Dr. Brian Todd Hefner, Principal Investigator

Subj: ONR Grant N00014-16-1-2999, "TREX13 Transmission Loss and Sea Floor Scattering Analysis and Modeling"

Encl: (1) Final Technical Report
(2) Publication "Reverberation due to a moving, narrowband source in an ocean waveguide" J. Acoust. Soc. Am. 146 (3), September 2019
(3) SF298 form

Please see the enclosures listed above for the subject grant, "TREX13 Transmission Loss and Sea Floor Scattering Analysis and Modeling". Enclosure (1) is the final report that closes the subject grant, enclosure (2), the final publication from the grant, with an attached SF298 form as enclosure (3).

cc: ONR Seattle – Ms. Ozma Ragan (ozma.ragan@navy.mil) and
Ms. Naomi Roberson (naomi.roberson.ctr@navy.mi)
Naval Research Laboratory, Code 5596, reports@library.nrl.navy.mil
Defense Technical Information Center: dtic.belvoir.ecm.mbx.tr@mail.mil
University of Washington – Office of Sponsored Programs Closeout Coordinator
Grant & Contract Closeout Coordinator, APL-UW

TREX13 Transmission Loss and Sea Floor Scattering Analysis Modeling Final Report

Brian Todd Hefner
Applied Physics Laboratory, University of Washington
1013 NE 40th Street, Seattle, WA 98105 USA
phone: (206) 616-7558 fax: (206) 543-6785 email: hefner@apl.washington.edu

Award Number: N00014-16-1-2999

LONG-TERM GOALS

The long-term goal of this project is to understand how the environment impacts mid-frequency (1-10 kHz) transmission loss (TL) and reverberation level (RL). Through experiments which simultaneously measure TL and RL with extensive environmental characterization, those environmental properties which most impact target detection can be identified and incorporated into sonar performance prediction models.

OBJECTIVES

There are two main objectives to the work conducted under this project. The first was to examine how the TL measurements collected during TREX13 are impacted by the spatial and temporal variations in the environment and how these impacts are manifested in the measured RL. The second objective was to develop a coupled propagation and scattering model to understand the Doppler-shifted reverberation generated by a towed source during the experiment and to determine if these measurements can be used as a tool to characterize sea floor scattering mechanisms.

APPROACH

The proposed work in this project was to develop and test techniques to exploit the Doppler-shifted signals to improve beam-forming results on the TREX13 limited-aperture arrays, catalog and develop a database of TL transmissions to complement that developed previously for the RL measurements, and use the VLA data to test models of bistatic scattering based on environmental characterization at the TREX13 site. The proposed research was as follows:

1. Using the towed-source data collected on the VLAs during TREX13, utilize the Doppler-shifted signals to enhance the output and interpretation of a beam-former applied to the data. Two sets of data were to be examined: the narrow-band, 15 s tone data and the broad-band, 15 s LFM data. Each of these datasets have obvious tradeoffs between time-resolution and signal-to-noise, each of which may be useful in understanding and modeling the beam-former output.
2. Using the reverberation cataloging and classification work conducted by Dr. Jie Yang as a guide, identify and isolate the corresponding VLA receptions to create a parallel catalog of transmission measurements. This collection can be used to further constrain reverberation models by providing synchronous TL and RL measurements for data/model comparisons. In collaboration with Drs. Tang and Yang and software engineer Linda Buck, this catalog was to

be developed into a database of reverberation and VLA receptions that can be used by other researchers.

3. Use the results of the towed-source analysis in Task #1 to study the evolution of the TL between the RAS and the VLAs under changing surface and water-column conditions. This work was to be conducted in conjunction with Dr. Eric Thorsos who is being funded separately by ONR to continue development of transport theory for propagation and reverberation.
4. Using the beam-forming techniques developed above, focus on the reverberation measured on the VLAs during the towed-source measurements with the goal of identifying the bistatic scattering contributions from the sediment. This was to be complemented by modeling of the scattered field using the roughness and volume scattering cross-sections measured during TREX13.

WORK COMPLETED AND RESULTS

Task 1 and 4: Utilization of the Doppler-shifted signals from TREX13 and identifying the bistatic scattering contributions from the sediment.

A model for the bistatic reverberation associated with seafloor scattering of sound from a moving, narrowband source in an ocean waveguide was developed and published in the Journal of the Acoustical Society of America [1]. The model uses a single scattering approximation. The field propagating from the source to a seafloor scattering patch was modelled using a ray approximation, the field propagating from the patch to the receiver was modelled using modes, and the scattering into each mode was determined using ray-mode analogies. The model was applied to the narrowband 15 s tones transmitted from the towed source to the two vertical line arrays deployed by Dr. William Hodgkiss during TREX13. The model compared very favorably to the data using the sediment parameters measured during the experiment as inputs (Figure 1).

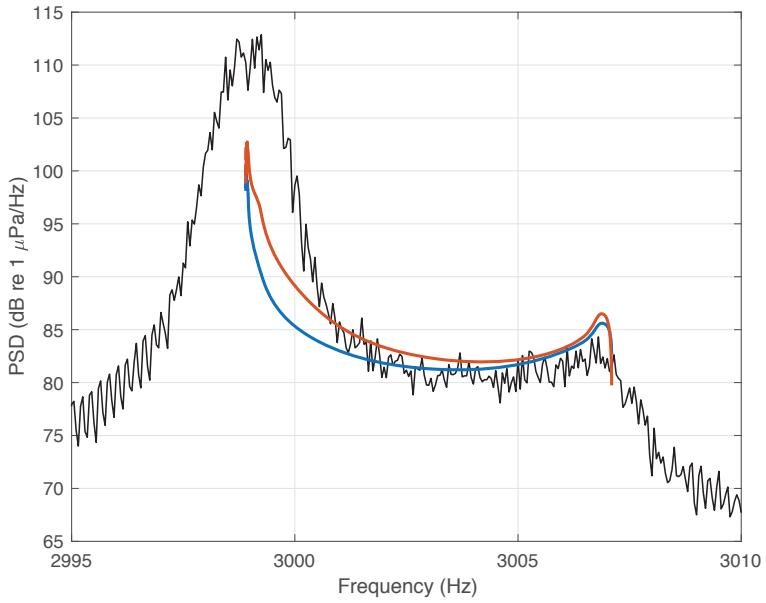

Figure 1: Comparison of the Doppler reverberation model to the power spectral density (PSD) measured on the vertical line array for a source being towed away at 2.1 m/s along the TREX13 main reverberation track. The model used parameters measured during TREX13 with the scattering cross-section given by Lambert's law (dark blue line) and small-roughness perturbation theory (light red line)

Task 2: Create a catalog transmissions received on the VLAs during TREX13

The data measured on each element of the three VLAs deployed during TREX13 were provided by Dr. William Hodgkiss to APL-UW for this project. The VLAs recorded continously during the period from 22 April to 11 May. During this time, a bottom-mounted ITC-2015 source periodically transmitted 1-s long CW and LFM signals in the 2-4 kHz band while a bottom-mounted triplet array was used to measure the reverberation. Under a previously-funded effort, Dr. Jie Yang cataloged and classified the reverberation measured on the triplet array during this period [2]. Using the results of that effort, the corresponding receptions on the VLAs were extracted from the Scripps dataset. The resulting database of transmission and reverberation measurements makes it possible compare simultaneous measurements of transmission loss and reverberation level to constrain the ongoing reverberation modeling efforts (Figure 2).

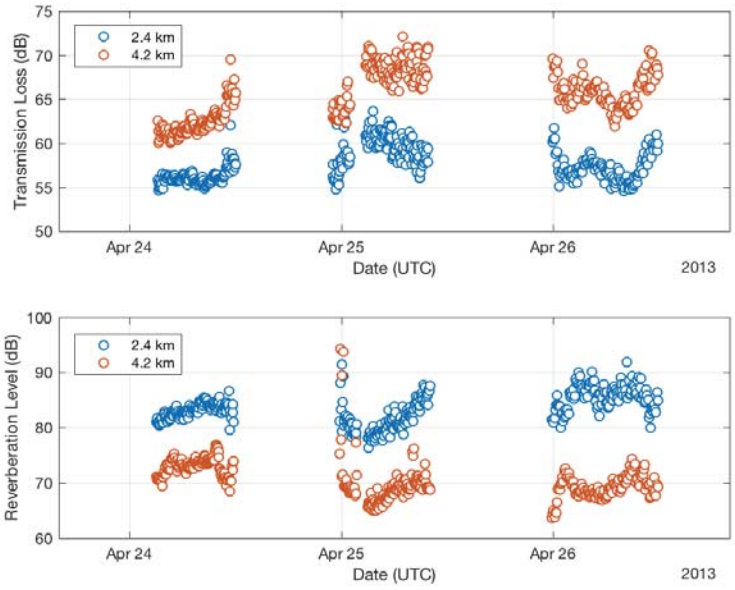

Figure 2: Comparison of the transmission loss measured on the VLAs at 2.4 km (blue) and 4.2 km (red) along the main reverberation track (upper panel) to the reverberation levels measured at the same ranges (lower panel).

Task 3: Study the evolution of the TL between the RAS and the VLAs under changing surface and water-column conditions

The temporal dependence of the TREX13 environment can be divided into two different time frames separated by the passage of a storm in the middle of the experiment. Prior to the storm, the seas were calm and the sound speed profile (SSP) had a thermocline of 3°C that formed a duct just above the seafloor. The thermocline depth could vary by as much as 5 m over the course of a day and this variation in the SSP was found to be the driver of TL variations prior to the storm. An example of these variations is shown in the upper panel of Figure 2. After the storm, the SSP was predominantly isotropic and the changes in TL can be associated with the rough sea surface and its gradual decay as seen in Figure 3.

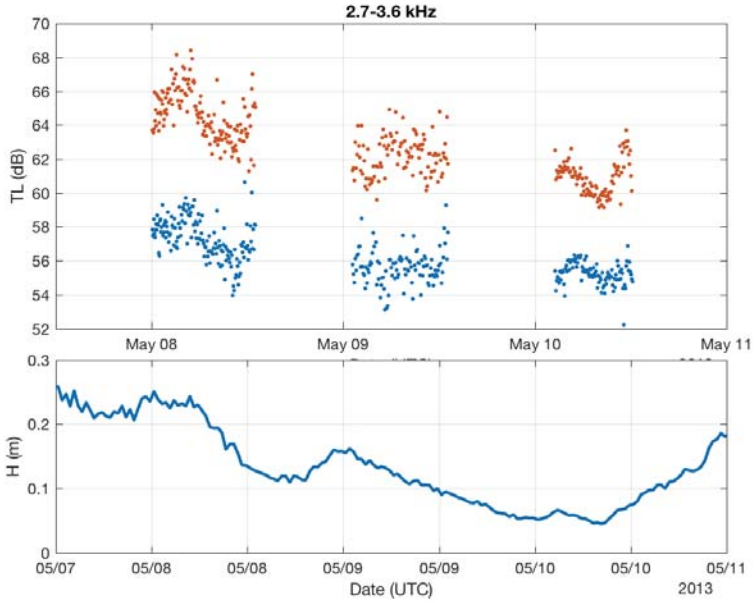

Figure 3: Comparison of the transmission loss measured on the VLAs at 2.4 km (blue) and 4.2 km (red) along the main reverberation track (upper panel) to the RMS surface height measured by an upward-looking acoustic waves and current (AWAC) sensor.

While it was possible at the outset to demonstrate a qualitative dependence of the transmission loss on both the sound speed profile and the sea surface roughness, uncertainties in the environmental characterization made it difficult to model this dependence. In particular, despite local measurements of the seafloor properties which indicated that it was predominantly sand with an attenuation of 0.5-0.7 dB/λ [3-5], inversions of the range-dependent transmission loss indicated that the sediment was either softer than the direct measurements indicated or the attenuation of the sand should be much higher (1.5 dB/λ) (Figure 4).

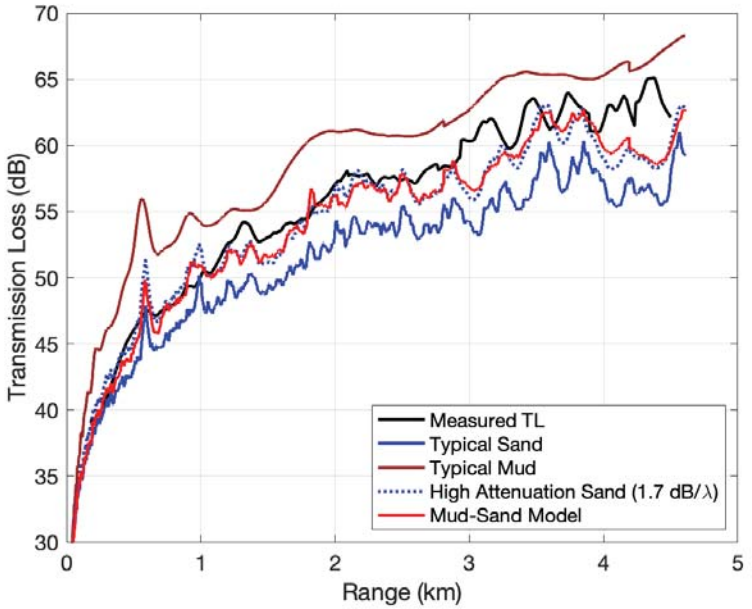

Figure 4: Transmission loss measured for a 3.5 kHz tone. Also shown are the transmission loss model results for a typical sand (blue), typical mud (brown), high-attenuation sand (blue-dotted), and the mud-sand geoacoustic model.

The inversions discussed above assumed a uniform sediment along the track, an assumption that we initially felt was supported by the lack of any clear range-dependence to the TL. Direct measurements of acoustic scattering, reflection, and sediment propagation at the site also found that although there were narrow mud patches along the main reverberation track, these mud patches accounted for less than 20-30% of the seafloor along the track. Recent efforts to test this hypothesis have found that while the sediment is predominantly sand, these narrow patches of mud may actually have a significant impact on the transmission loss.

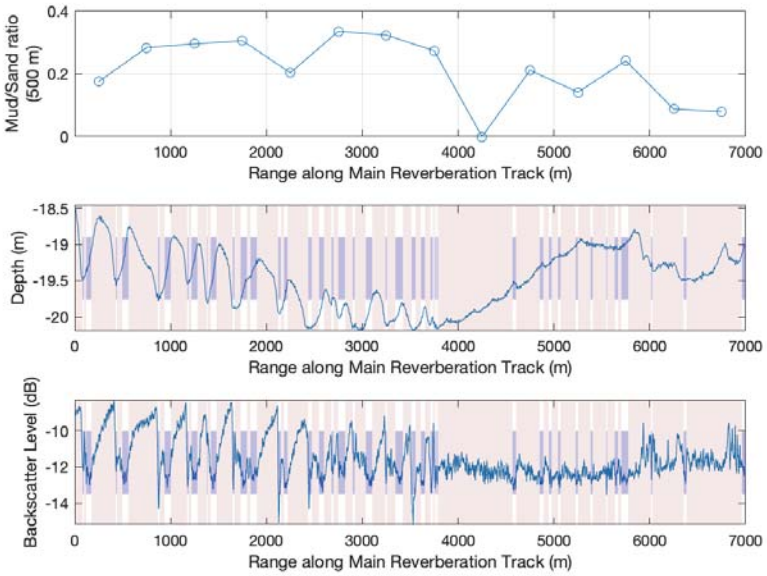

Figure 5: (Top) Ratio of mud to sand over 500 m lengths of the sediment along the TREX13 main reverberation track. The estimated locations of mud (purple) and sand (red) compared to (middle) the bathymetry and (bottom) the multibeam backscatter levels along the track.

Figure 5 shows a rough estimate of the locations of mud along the main reverberation track based on the scattering levels measured using a high-frequency multibeam sonar and reflection measurements at 3.5 kHz. The ratio of mud to sand varies but is roughly 25%. When this range-dependence is introduced into the transmission loss modelling using the parabolic equation, the model provides a good match to the data without assuming any anomalously large attenuation for the sediment. The lack of range-dependence in the TL despite the range-dependence of the sediment properties can be understood through the results of a numerical experiment shown in Figure 6. Transmission loss was modeled as a function of range using PE in an isovelocity, constant-depth water column with a sand seafloor with areas of mud such that the ratio of mud to sand over the entire 7 km length was held constant at 20%. For each run, the number of mud patches was doubled and distributed uniformly along the length of the simulation. When the number of patches is low (<16), the transmission loss shows clear jumps as the field propagates over the softer sediment. However, once the number of patches grows large enough, the TL curve becomes smooth and lacks any clear range-dependence. This model of the seafloor is currently being refined through a reevaluation of the environmental measurements made during the experiment and we expect to publish the results of the analysis and modeling work in an upcoming ONR-funded effort.

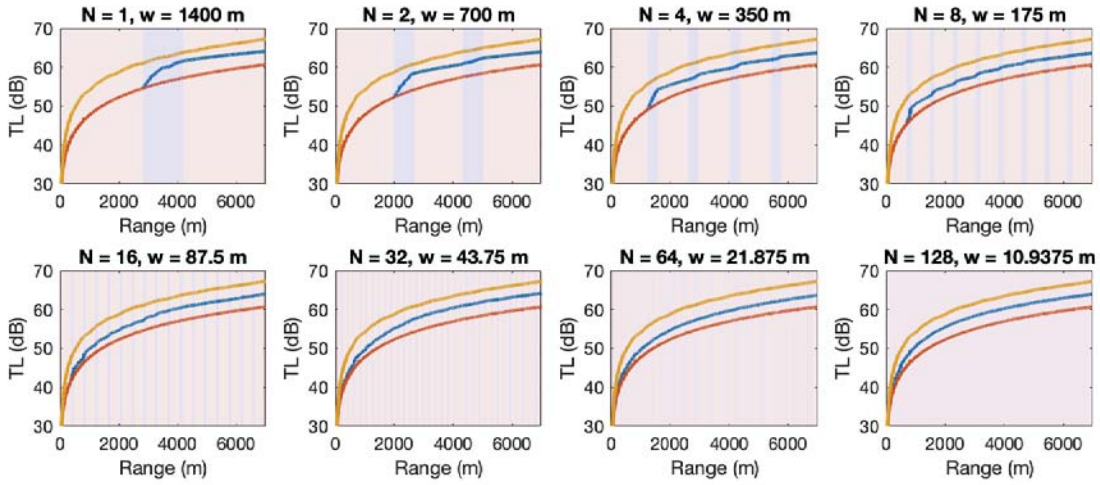

Figure 6: Depth-averaged transmission loss for an isovelocity waveguide at 3.5 kHz with a sediment composed of sand (light red) and mud (light purple). In each plot, the ratio of mud to sand is held fixed while the number of mud regions is doubled in each successive plot. The blue curve in each plot is the TL for the range-dependent mud and sand sediment. The yellow curve is for a range-independent mud sediment and the red curve is for a range-independent sand sediment.

This model of the transmission loss for TREX13 has important implications for our understanding of reverberation at the site. Reverberation modelling efforts to this point have also assumed a uniform sand sediment and when combined with rough surface scattering using the roughness spectra measured at the site, the reverberation models appear to match the data (Figure 7) [6]. This neglects the transmission loss measurements as well as measurements of the volume scattering at the site. If the mud is accounted for in the transmission loss and the volume scattering is neglected, the reverberation is significantly underestimated. The data/model comparison is recovered when the measured volume scattering is also added into the reverberation model.

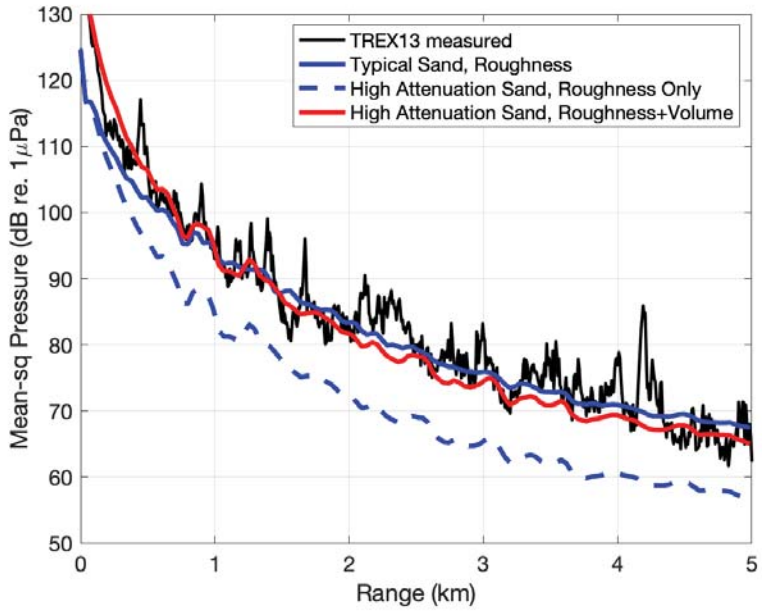

Figure 7: Reverberation measured for a 1 sec, 3.4-3.5 kHz pulse. Also shown are the reverberation model results for a typical sand seafloor with the measured roughness scattering (blue), a high-attenuation sand seafloor with the measured roughness scattering (blue dashed), and a high-attenuation sand seafloor with the extrapolated volume scattering.

Incorporating the mud/sand range-dependence into the model of the TREX13 seafloor reconciles the results of the transmission loss, reverberation, roughness, and volume scattering measurements. The goal of the experiment was to "measure mid-frequency shallow water reverberation with full companion environmental measurements so model/data can be compared without ambiguity." While there is still work to be done to fully understand and model the data from TREX13, we have made significant strides in realizing this goal.

IMPACT/APPLICATIONS

Through this project and several related ONR-funded efforts, many of the ambiguities identified in the prelimary TREX13 analysis have been resolved. The resulting dataset can now be used to assess deterministic and statistical variations in both transmission loss and reverberation under evolving environmental conditions. This dataset will be used in an upcoming project to assess the dominant evironmental impacts on mid-frequency sonar and assess the uncertainties in sonar performance predictions when these environmental factors are not included. The work to this point has largely ignored the targets deployed during the experiment and the environmental and acoustic models can be used in future work to assess predictions of signal excess under different environmental conditions.

RELATED PROJECTS

1. **N00014-17-1-2229: Shallow Water Reverberation: Data Analysis/Modeling and S. Korea Experiments**
   PI: Dajun Tang
   Period of Performance: 3/1/2017-2/29/2021

REFERENCES

1. Hefner, B. and Hodgkiss, W. (2019) “Reverberation due to a moving, narrowband source in an ocean waveguide”, J. Acoust. Soc. Am. 146(3), 1661-1670.
2. Yang, J., Tang, D., Hefner, B., Williams, K., and Preston, J. (2018). “Overview of Midfrequency Reverberation Data Acquired During the Target and Reverberation Experiment 2013,” IEEE J. of Ocean. Eng. **43**(3), 563-585.
3. Dall'Osto, D., Choi, J., and Dahl, P. (2016) “Measurement of acoustic particle motion in shallow water and its application to geoacoustic inversion,” J. Acoust. Soc. Am., **139** (1), 311-319.
4. Yang, J. and Tang, D. (2017) “Direct Measurements of Sediment Sound Speed and Attenuation in the Frequency Band of 2–8 kHz at the Target and Reverberation Experiment Site,” IEEE J. of Ocean. Eng. **42**(4), 1102-1109.
5. Holland, C., Pinson, S., Smith, C., Hines, P., Olson, D., Dosso, S., and Dettmer, J. (2017) “Seabed Structure Inferences From TREX13 Reflection Measurements,” IEEE J. of Ocean. Eng. **42**(2), 268-288.
6. Ellis, D., Yang, J., Preston, J., and Pecknold, S. (2017) “A Normal Mode Reverberation and Target Echo Model to Interpret Towed Array Data in the Target and Reverberation Experiments,” IEEE J. of Ocean. Eng. **42**(2), 344-361.

PUBLICATIONS

1. Hefner, B. and Hodgkiss, W. (2019), “Reverberation due to a moving, narrowband source in an ocean waveguide”, J. Acoust. Soc. Am. 146(3), 1661-1670.

Reverberation due to a moving, narrowband source in an ocean waveguide

Brian T. Hefner[1,a)] and William S. Hodgkiss[2]
[1]*Applied Physics Laboratory, University of Washington, 1013 NE 40th Street, Seattle, Washington 98105, USA*
[2]*Scripps Institution of Oceanography, University of California, San Diego, La Jolla, California 92093, USA*

(Received 16 April 2019; revised 17 August 2019; accepted 22 August 2019; published online 20 September 2019)

In this paper, a model for the bistatic reverberation associated with seafloor scattering of sound from a moving, narrowband source in an ocean waveguide is developed. Studies of the Doppler effect for moving sources in waveguides have typically focused on the forward propagating field where the Doppler shift leads to a splitting or broadening of the received spectrum. In contrast, the contributions to the scattered field come from all directions and as a consequence the spectrum of the received energy is spread across the entire range of Doppler-shifted frequencies possible for the speed of the source. The model developed here uses rays for the incident field, ray-mode analogies for the scattering, and normal modes to propagate the scattered field to the receiver. Results from this model are compared with data collected using a towed source during the Target and Reverberation Experiment 2013. The possible applications of this Doppler reverberation for seafloor characterization are also considered.
https://doi.org/10.1121/1.5126023

[SED] Pages: 1661–1670

I. INTRODUCTION

The detection of targets using active sonar in the shallow water environment is often reverberation limited. One technique used to isolate the target from the reverberation is to exploit the Doppler shift of the target return. This assumes that the target is moving relative to the scatterers in the environment. This assumption can break down in the presence of a rough sea surface where spectral spreading of the reverberation from the surface can be induced by both the wave motion itself (Brown and Frisk, 1974; Lynch and D'Spain, 2012; Wild and Joyce, 1995) and by the motion of entrained bubbles (McCammon and McDaniel, 1990). This can increase the relative importance of sea surface scattering in sonar performance prediction in shallow water environments where seafloor scattering is typically greater than scattering from the sea surface (Thorsos *et al.*, 2011). When the sonar itself is also moving, the Doppler of the transmitted signal will be present in the seafloor scattering contribution to the reverberation. If the source has a narrow beampattern, the Doppler shifts across the beam have been observed to lead to beating in the time series response of the sonar (Hurdle *et al.*, 1964). For a source with a broad beampattern, the Doppler shifts of the outgoing sound will broaden the frequency response of the seafloor reverberation. This spread in the Doppler spectrum was observed in a set of bistatic reverberation measurements collected in the Gulf of Mexico in 2013. This paper discusses those measurements and develops a model of the Doppler spectrum of the seafloor reverberation.

The measurements were made as part of the Target and Reverberation Experiment conducted in the Spring of 2013 (TREX13). The primary goal of the experiment was to simultaneously measure mid-frequency (2–10 kHz) reverberation and transmission loss with extensive environmental characterization (Yang *et al.*, 2018). As part of the effort to measure transmission loss at the site, two vertical line arrays of receivers were deployed and a source transmitting 15-s long tonals was towed at mid-water depth past each array. Details of these measurements are given in Sec. II. While the main peak in the received energy occurred at a Doppler-shifted frequency consistent with the velocity of the source relative to the array, $f_0 + \Delta f$, where f_0 is the transmitted frequency and Δf is the Doppler shift, there is an appreciable amount of energy distributed in the band between $f_0 - \Delta f$ and $f_0 + \Delta f$.

This spectral response is due to sound leaving the source in directions away from the direct source-to-receiver path and being scattered back to the array. While the direct path propagation will have a Doppler-shifted frequency corresponding to the relative velocity between the source and the array, the reverberation will occur at Doppler-shifted frequencies corresponding to the velocity of the source relative to the scattering location in the environment. The sound scattered from this location to the array will then have the same Doppler-shifted frequency as the incident sound regardless of the direction of the array from the scatterer. For the nearly omnidirectional source used in the experiment, the reverberation will therefore cover the band of Doppler-shifted frequencies defined by $f_0 \pm \Delta f$. A similar effect is observed in airborne, pulse Doppler radar where the side lobe returns can be spread across the Doppler space (Skolnik, 2001). This issue has obviously received more attention in the radar community since aircraft speeds are more than an order of magnitude faster than ship speeds and the spread in Doppler is much more significant as a result.

a)Electronic mail: hefner@apl.washington.edu

The modeling approach used here is based on the reverberation models developed by Bucker and Morris (1968) and Ellis (1995) and is illustrated in Fig. 1. The incident field is modeled using a ray approximation and takes into account the Doppler shift of the field. The scattering is modeled using ray-mode analogies and the propagation of the scattered field is described using normal modes. The model is developed in Sec. III and comparisons of the model to data are given in Sec. IV. Section V discusses the implications of the Doppler broadening of the seafloor reverberation for possible applications of the effect for environmental characterization and sonar performance prediction.

II. MEASUREMENTS AT TREX13

The Target and Reverberation Experiment was conducted in the Spring of 2013 (TREX13), 2 km off the coast of Shell Island near Panama City Beach, Florida. The primary goal of the experiment was to simultaneously measure mid-frequency (2–10 kHz) reverberation and transmission loss with extensive environmental characterization (Yang *et al.*, 2018). Reverberation was primarily measured using a bottom-mounted source and horizontal line array which were deployed from the moored R/V Hugh R. Sharp at the center of the experiment site. In order to limit the area within which environmental characterization was needed, the reverberation analysis focused on an area along a bearing of 129° which was designated as the "main reverberation track." The location of the R/V Sharp and the bathymetry measured along the main reverberation track are shown in Fig. 2.

To measured transmission loss, two vertical line arrays (VLAs) were deployed along the main reverberation track at ranges of 2.4 and 4.2 km from the reverberation source (see Fig. 2). Each array consisted of 32 elements equally spaced at increments of 0.2 m for a total aperture of 6.2 m. The lowest element was located 5 m above the seafloor. The VLAs were autonomous, self-recording systems with a sampling rate of 25 kHz for each element. In order to measure acoustic propagation as a function of range along the main reverberation track, a mid-frequency source was deployed from the R/V Walton Smith and suspended in the middle of the water

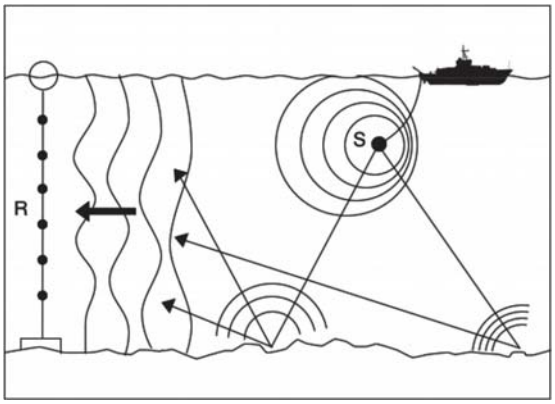

FIG. 1. Illustration of the scattering of the Doppler-shifted field and the approach used to model the reverberation from a moving source. The Doppler-shifted sound is modeled using a ray approximation and the sound is scattered at the seafloor into normal modes which propagate to the receivers.

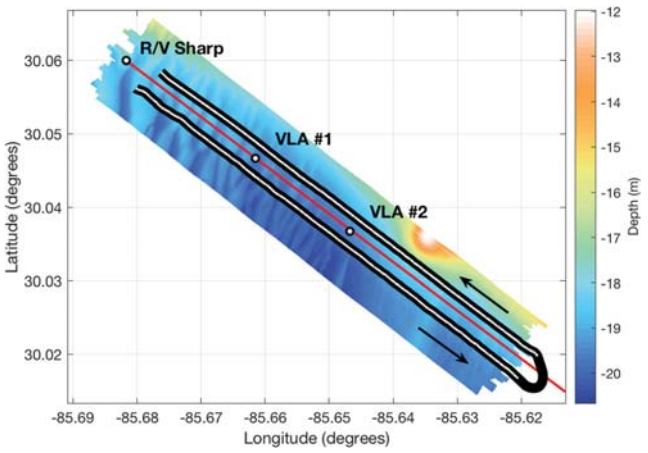

FIG. 2. (Color online) Map of the TREX13 experiment site showing the locations of the moored R/V Sharp, VLA #1, and VLA #2. The bathymetry is shown for the "Main Reverberation Track," a region of the seafloor centered on a bearing of 129° extending from the location of the R/V Sharp and indicated by the red line. The path of the R/V Walton Smith during the source tow is indicated by the thick black line. The source transmissions were made along the portions of the path indicated in white.

column. The source was towed along the path shown in Fig. 2. The source was an ITC-2015 which transmitted a tonal comb consisting of 15 s-long continuous wave (CW) signals from 1503 to 4003 Hz in 500 Hz increments. The analysis and modeling presented below will focus on the $f_0 = 3003$ Hz tone which was transmitted with a source level of 173.2 dB re μPa @ 1 m. During the tow, the signal was transmitted with a 50% duty cycle, i.e., 30 s between transmissions.

The data recorded on each element during the tow was partitioned into 30 s long segments which captured the received tones from each transmission. This 30 s long time series of pressure was Fourier transformed and the absolute value squared was taken. The mean was taken across the 32 elements of the array and divided by the transmission time of 15 s to obtain the power spectral density (PSD). The PSD received on the VLAs during the out-going tow (away from the R/V Sharp) as a function of distance from the closet point of approach (CPA) for each array is shown in Fig. 3.

The average speed of the R/V Smith, $\langle|v|\rangle$, during the source tow was 2.0 m/s which produces a direct path, Doppler-shifted frequency of $f_0(1 + \langle|v|\rangle/c_w) = 3007$ Hz when the source is moving towards the receiver and $f_0(1 - \langle|v|\rangle/c_w) = 2999$ Hz when the source is moving away, where c_w is the water sound speed. The frequency of the peak in the power spectral density in Fig. 3 is consistent with these extremes when the source is far from the receiver and transitions through the tonal frequency as the source passes through the CPA. While the direct path from a moving source in a waveguide should broaden due to the Doppler shifts of the individual propagating modes, the broadening of the direct arrival peaks in Figs. 3 and 4 is wider than expected given the frequency and speed of the source. This additional broadening could be due to small accelerations of the source during the tow. Variations in the speed of the source on the order of 0.2 m/s is enough to account for the broadening of the direct arrival observed in Fig. 4. Another source of the broadening could be additional Doppler shifts

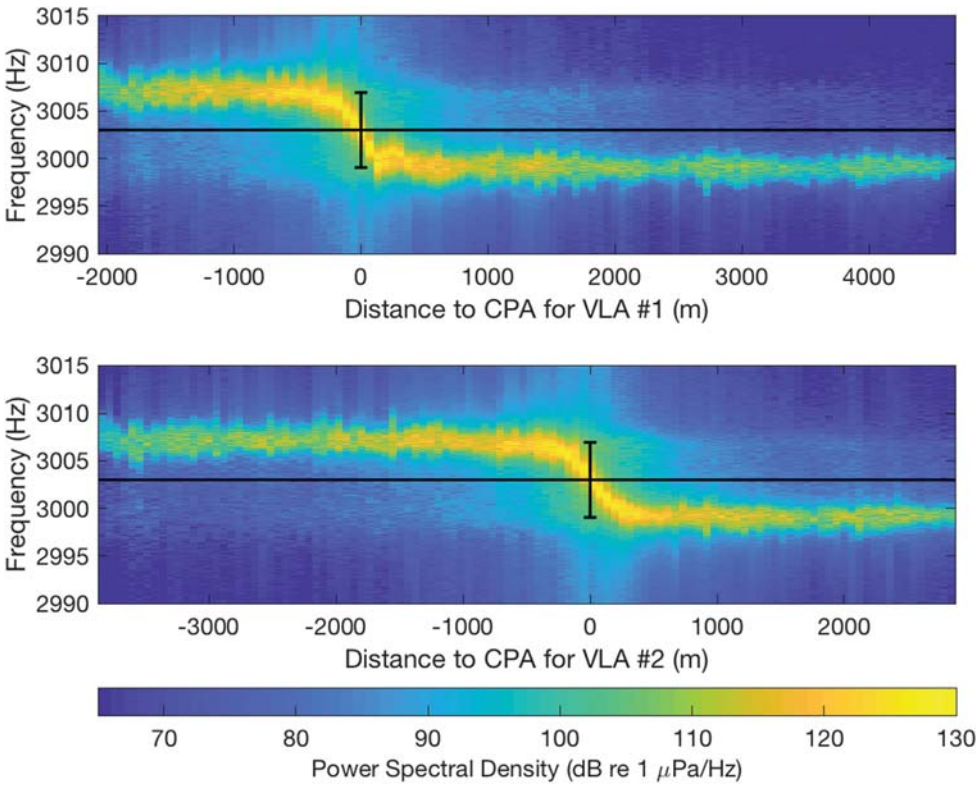

FIG. 3. (Color online) The average power spectral density measured on VLA #1 (top panel) and VLA #2 (bottom panel) for each transmission as the source is towed past the arrays along the outgoing path. The distance is measured relative to the closest point of approach (CPA) of the source to the VLAs. The black horizontal line indicates the frequency of the transmitted tonal (3003 Hz) while the vertical bars indicate the maximum and minimum Doppler-shifted frequencies (2999 and 3007 Hz) for the mean tow speed of 2.0 m/s.

imposed by the motion of the sea surface during the tow. The root mean square (RMS) height of the sea surface varied over 0.10–0.15 m during the towed and stationary transmissions.

In addition to this direct path energy, throughout the tow there is also energy arriving at all frequencies within the band defined by these two Doppler frequencies (2999 and 3007 Hz). This is seen more clearly in Fig. 4 which shows the PSD measured on VLA #1 when the source is 2.1 km from the CPA and moving with a velocity of −2.1 m/s. At this range and velocity the direct arrival has a Doppler-shifted frequency of 2998 Hz and spectral level of 112 dB. The energy spread across the 2998−3008 Hz band is clearly seen and while it is roughly 30 dB below the direct path level, it is still well above the noise floor which is at 67 dB. As explained in the Sec. I and in more detail in Sec. III, this broad spectral response across the entire Doppler band is due to sound leaving the source in directions away from the direct source-to-receiver path and being scattered back to the array.

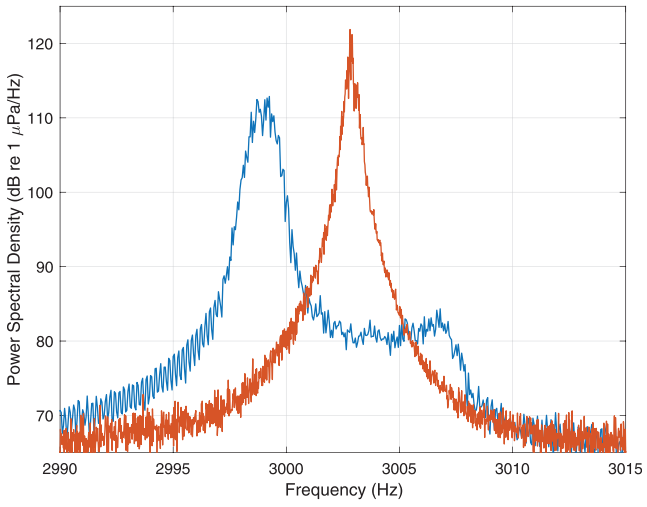

FIG. 4. (Color online) The power spectral density measured on a vertical line array when the source was being towed at –2.1 m/s at a range of 2.1 km along the main reverberation track (dark blue). Also shown is the PSD when the source was transmitting from a stationary position ($v = 0$ m/s) at a range of 2.1 km (light red). The transmitted signal was a 15-s-long, tone at 3003 Hz.

III. DOPPLER REVERBERATION MODELING

In this section, we will develop a model for the bottom reverberation produced by a CW source moving through an ocean waveguide. Prior to developing this model, it is useful to conceptually distinguish the approach used to model the reverberation in the frequency domain from the approach typically used to model reverberation in the time domain. Figure 5(a) shows an idealized representation of the bistatic reverberation measured as a function of time for a broadband pulse transmitted from a stationary source. The time series of the intensity peaks with the direct arrival which is then followed by a decay in intensity as a function of time (Ellis, 1993). At any given time, t_0, the field measured at the receiver is due to scattering from an elliptical patch of the seafloor for which the propagation path from the source to

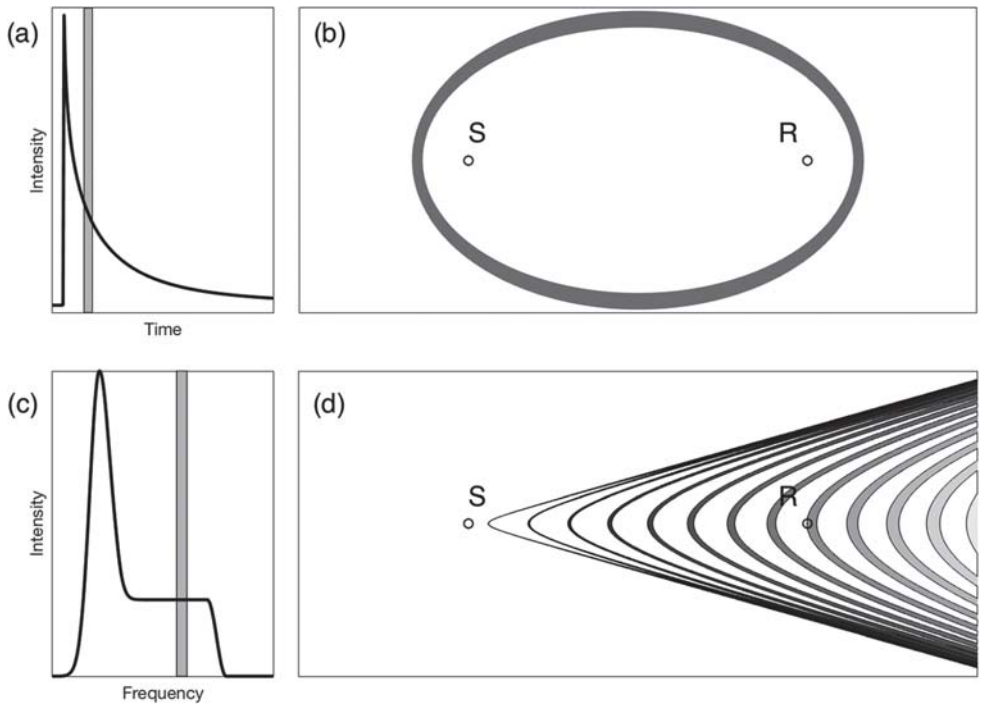

FIG. 5. (a) Bistatic reverberation measured in the time domain for a broadband pulse. (b) The elliptical patch from which the scattered field arrives at the time interval indicated by the shading region in (a). (c) Bistatic reverberation measured in the frequency domain for a moving, narrowband pulse. (d) The hyperbolic patches which scatter sound to the receiver in the frequency band indicated by the shaded region in (c). The sources are shown as "S" in (b) and (d) while the receivers are indicated by "R." The gray vertical bar in (a) denotes the arrival time of sound scattered from the elliptical patch in (b). The gray vertical bar in (c) denotes the frequency of the sound scattered from the shaded patches in (d).

the seafloor, r_1, and from the seafloor to the receiver, r_2, satisfies $t_0 = (r_1 + r_2)/c_w$. An example of this elliptical scattering patch is shown in Fig. 5(b).

The reverberation measured as a function of frequency for a moving, narrowband source is shown in Fig. 5(c). In this example the source is moving away from the receiver and the large spectral level corresponds to the direct arrival. Sound leaving the source in directions other than those corresponding to the direct path will experience different Doppler-shifts and scatter from the seafloor. This scattered energy can then propagate back to the receiver and contribute to the spectral levels across the Doppler band. The Doppler-shifted frequency, f, is associated with sound leaving the source at some angle θ_x, the angle between the outgoing acoustic wave vector and the velocity vector of the source, which will be assumed to be aligned with the x axis, and expressed as

$$f = f_0\left(1 + \frac{v_x}{c_w}\cos\theta_x\right), \tag{1}$$

where v_x is the velocity in the direction of motion of the source. The surface of constant frequency forms a cone about the velocity vector and the intersection of this cone with the seafloor defines the scattering patch which is a hyperbola on the seafloor. In the case of a source and receiver above a half-space, a single hyperbolic scattering patch would exist for each frequency. In a waveguide, the sound will reflect multiple times from the seafloor and sea surface and as a result multiple scattering patches will exist for a given Doppler-shift as shown in Fig. 5(d).

Since the source will initially be assumed to be omnidirectional, the incident grazing angles on the seafloor will range from 0° to 90°. In order to account for the sound at very steep grazing angles, the incident field will be modeled using a ray approximation. Also, since we are interested only in the intensity of the reverberation, spherical wave effects at the bottom reflection will be neglected and a plane wave approximation will be used. For the scattered field, we will use a single scattering approximation; the sound can scatter into a range of angles which will then propagate without further scattering down the waveguide. To account for the angular spread in scattered energy, the propagating field will be modeled using normal modes. The scattering into the modes will be determined using ray-mode analogies and the scattered field is assumed to be dominated by sound traveling at grazing angles below the critical angle. Hence only the trapped modes will be used.

The source is assumed to be omnidirectional, moving at height, H, above the seafloor with constant velocity in the x-direction, and transmitting a continuous tone of frequency, f_0. The ocean waveguide is treated as isovelocity with sound speed, c_w, and is range-independent with water depth, D. The seafloor sediment is characterized by the sediment/water density ratio, ρ, the sediment sound speed, c_s, and the ratio of the imaginary to real wave number in the sediment, δ. The sea surface is assumed to be flat, while the seafloor has small-scale roughness at its interface and heterogeneities in its volume, both of which can contribute to the bistatic scattering cross-section,

$$\sigma_b(\theta_s, \phi_s, \theta_i) = \sigma_r(\theta_s, \phi_s, \theta_i) + \sigma_v(\theta_s, \phi_s, \theta_i), \tag{2}$$

where σ_r and σ_v are the roughness and volume scattering cross sections per unit area, respectively. The incident grazing angle, θ_i, the scattered grazing angle, θ_s, and the bistatic angle, ϕ_s, follow the convention used in Jackson and Richardson (2006, Fig. 2.4).

As discussed above, the cones of constant frequency defined in Eq. (1) intersect the seafloor to form hyperbolas described by

$$x = \frac{1}{\tan\theta_x}\sqrt{y^2 + H^2}, \tag{3}$$

as shown in Fig. 6. While these hyperbolas are defined for the direct path from the source to the seafloor, sound which reflects from the sea surface prior to reaching the seafloor can be modeled using an image source at height, $H_1 = (D - H) + D$, above the seafloor. After multiple reflections from the seafloor, the incident sound can be modeled using an image source at height,

$$H_{nm} = (-1)^n H + (n + m)2D, \tag{4}$$

where $n = 0$ for sound that reflects first with the seafloor after leaving the source, $n = 1$ for sound that reflects first from the sea surface, and $m = 0, 1, 2,\ldots$ is the number of reflections from the seafloor. For these image sources, the associated hyperbolas for the sound incident on the seafloor become

$$x_{nm} = \frac{1}{\tan\theta_x}\sqrt{y^2 + H_{nm}^2}. \tag{5}$$

Assuming that the source is transmitting at intensity, I_0, and using a plane-wave approximation, the intensity of the sound at the seafloor is

$$I_{nm} = \frac{I_0 |V_{nm}|^{2m}}{r_{nm}^2(y)}, \tag{6}$$

where V_{nm} is the plane-wave reflection coefficient,

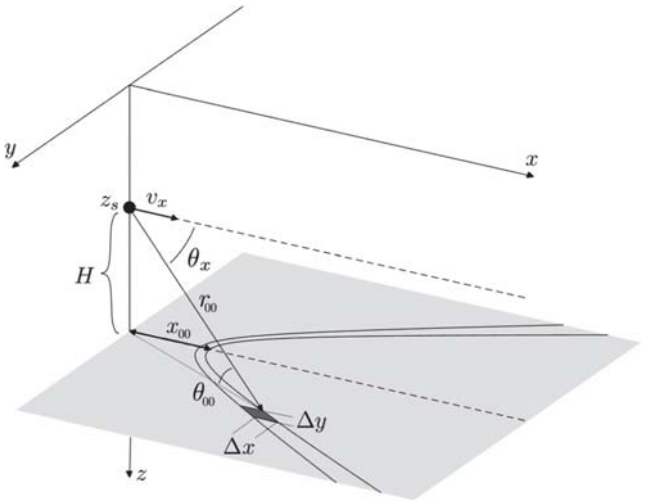

FIG. 6. Geometry of the sound directly incident on the seafloor for Doppler frequency, f, and the associated scattering patch for the frequency band from f to $f + \Delta f$.

$$V_{nm} = \frac{\rho c_s \sin\theta_{nm} - c_w \sin\theta_p}{\rho c_s \sin\theta_{nm} + c_w \sin\theta_p}, \tag{7}$$

$$\sin\theta_p = \sqrt{1 - \frac{c_s}{c_w}\sin\theta_{nm}}, \tag{8}$$

the incident grazing angle is given by

$$\sin\theta_{nm} = \frac{H_{nm}}{r_{nm}}, \tag{9}$$

and the distance from the real or image source to a point along the hyperbola on the seafloor is

$$r_{nm}^2 = \frac{y^2 + H_{nm}^2}{\sin^2\theta_x}. \tag{10}$$

To use the cross-section given by Eq. (2) to determine the scattering, a narrow band of frequencies, Δf, at the Doppler-shifted frequency will be used to determine the size of the scattering patch on the seafloor. For this band of frequencies, the change in Doppler can be written as

$$f + \Delta f = f_c\left(1 + \frac{v_x}{c_w}\cos(\theta_x + \Delta\theta)\right). \tag{11}$$

Assuming that the bandwidth is small and $\Delta\theta \ll \theta_x$, the range of angles subtended by this band can be approximated as

$$\Delta\theta \approx \frac{\Delta f c_w}{f_c v_x}\frac{1}{\sin\theta_x}. \tag{12}$$

The width of the seafloor scattering patch corresponding to this range of angles can be found from Eq. (5) and can be written using the approximation in Eq. (12) as

$$\begin{aligned}\Delta x_{nm} &= \frac{1}{\tan(\theta_x + \Delta\theta)}\sqrt{y^2 + H_{nm}^2} \\ &\approx -\frac{\Delta f c_w}{f_c v_x}\frac{1}{\sin^3\theta_x}\sqrt{y^2 + H_{nm}^2}.\end{aligned} \tag{13}$$

The scattering strength at the patch can be calculated for a given scattering angle using the expression for the incident grazing angle given by Eq. (9) and the bistatic angle given by

$$\tan\phi_{nm} = \frac{y\tan\theta_x}{\sqrt{y^2 + H_{nm}^2}}. \tag{14}$$

The scattered field will be modeled using normal modes where the field due to a unit point source can be approximated as

$$p(r, z) \approx \sqrt{2\pi}e^{i(\pi/4)}\sum_j \Phi_j(z_0)\Phi_j(z)\frac{e^{ik_j r}}{\sqrt{k_j r}}, \tag{15}$$

where $\Phi_j(z)$ are the mode functions, k_j are the mode wavenumber, z_0 is the depth of the source, and r is the horizontal range from the source. To calculate the scattered field, we will follow the approach used by Ellis who used a ray-mode analogy to determine the amplitudes of the scattered modes

(Ellis, 1995). In that approach the modes were written as a sum of upward and downward propagating waves,

$$\Phi_j(z) = A_j(z)[e^{i\psi_j(z)} + Ve^{-i\psi_j(z)}], \tag{16}$$

where $A_j(z)$ is the amplitude of the mode function and $\psi_j(z)$ is the vertical phase function. For the general case of a horizontal stratified waveguide, the mode amplitude is depth dependent and the phase function can be expressed using the Wentzel–Kramers–Brillouin (WKB) approximation (Jensen *et al.*, 2011). For the isovelocity case considered here, the mode amplitude is depth independent and the vertical phase function becomes $\psi_j(z) = k_{jz}z$ where $k_{jz} = \sqrt{k^2 - k_j^2}$. In this case the mode amplitudes can be found from Eq. (16) and its derivative at the seafloor,

$$A_j = \frac{ik_{jz}\Phi_j + \frac{\partial \Phi_j}{\partial z}}{2ik_{jz}e^{ik_{jz}z}}. \tag{17}$$

The scattered intensity from a point, r_0, on the seafloor propagating in mode j can now be approximated as

$$|p_j(r,z)|^2 = 2\pi|A_j|^2|\Phi_j(z)|^2\frac{e^{-\alpha_j r'}}{k_j r'}, \tag{18}$$

where α_j is the imaginary part of k_j and $r' = |r - r_0|$.

Using the incident field given by Eq. (6), the scattering cross-section, and the incoherent sum of the scattered modes, the frequency-dependent reverberation can be expressed as

$$R(f) = \sum_n\sum_m 2\pi\int_{-\infty}^{\infty}\Delta x_{nm}I_{nm} \times \sum_j \sigma_{nmj}|\Phi_j(z)|^2|A_j|^2\frac{e^{-\alpha_j r'}}{k_j r'}dy, \tag{19}$$

where the integration is along the hyperbolas given by Eq. (5) and the width of the scattering patch is given by Eq. (13). Note that Δx_{nm}, I_{nm}, and σ_{nmj} are functions of the Doppler frequency and as a result, the angle θ_x. The modes are also a function of the Doppler frequency, but for the source speeds used in TREX13, a good approximation is to use the wavenumbers and mode functions at the source frequency, f_0, for all frequencies across the Doppler spectrum.

While the model assumes an omnidirectional source, it is straightforward to include a source with an arbitrary beam pattern by modifying the expression for the incident intensity given by Eq. (6). Assuming the directivity of the intensity, $B(\theta, \phi)$, is known and the grazing angle, θ, is positive for rays incident on the seafloor, the intensity can be rewritten as

$$I'_{nm} = \frac{B\left((-1)^n\theta_{nm}, \phi_{nm}\right)I_0|V_{nm}|^{2m}}{r_{nm}^2(y)}, \tag{20}$$

where the azimuthal angle is given by Eq. (14).

IV. DATA/MODEL COMPARISONS

To apply the model developed in Sec. III, we will use the TREX13 environmental parameters shown in Table I. A majority of these parameters were derived from measurements conducted at the TREX13 site. The mean water depth was found from the bathymetry survey conducted by DeMoustier and Kraft (De Moustier, 2014) and which is shown in Fig. 2. The water sound speed and density were determined from CTD casts along the main reverberation track. The sediment sound speed was measured by both time-of-flight (Yang and Tang, 2017) and by reflection measurements (Dall'Osto *et al.*, 2016; Holland *et al.*, 2017) and the mean value across these measurements has been used. Attenuation was also measured using these methods but, as is often the case for mid-frequency seafloor environmental characterization, the measured values have a significant amount of uncertainty. The measurements of attenuation at the site vary from 0.2 to 1.7 dB/λ and the value used in this paper, 0.5 dB/λ, falls within this range and is typical for sand sediments. The sediment density value is also typical of sand sediments and falls within the range of measurements made on diver cores collected at the site.

For the scattering cross-section, we will use only the roughness scattering cross-section. Measurements of the volume scattering indicate that there may be a homogenous sand layer over a sub-bottom layer within which a majority of the volume heterogeneities are confined. As a consequence the scattering from the volume is weak. For the roughness scattering cross sections, two scattering models will be considered here. This first is described by the well-known Lambert's law,

$$\sigma(\theta_s, \phi_s, \theta_i) = \mu \sin\theta_s \sin\theta_i, \tag{21}$$

where μ is the Lambert scattering strength. Note that this expression is typically used to model backscatter and has no dependence on the bistatic angle. Refined versions of Lambert's law have been developed in the past to improve the performance for bistatic scattering, particularly in the specular direction (Ellis and Crowe, 1991). However, since the contribution of the field scattered into the specular direction is obscured by the propagating field, we will use the original version given in Eq. (21). This bottom scattering model has been applied to the stationary, monostatic reverberation data collected at TREX13, and a value for the

TABLE I. Parameters describing the TREX13 environment.

Parameter	Value
Mean water depth (H)	19.6 m
Water sound speed (c_w)	1530 m/s
Water density (ρ_w)	1000 kg/m^3
Sediment sound speed (c_s)	1670 m/s
Sediment density (ρ_s)	2000 kg/m^3
Sediment attenuation (β)	0.5 dB/λ
Roughness spectral strength (w_2)	0.0015 m$^{4-\gamma_2}$
Roughness spectral exponent (γ_2)	4.23
Roughness characteristic length (L)	0.2 m
Lambert scattering strength (μ)	−31 dB

scattering strength of –31 dB was used to match the data (Ellis *et al.*, 2017). This value will also be used here.

The second roughness scattering model used here is first-order small-roughness perturbation theory. In addition to the sediment parameters, this model requires information about the roughness power spectrum of the seafloor. Direct measurements of the rough surface found that the spectrum could be described using a von Karman spectrum,

$$W_2(K) = \frac{w_2}{(K^2 + 1/L^2)^{\gamma_2/2}}, \tag{22}$$

where the spectral strength, w_2, and spectral exponent, γ_2, were found from a fit to the mean spectrum determined from measurements at multiple locations around the TREX13 site (Hefner, 2017). The characteristic length, L, was not directly measured and was arbitrarily chosen to prevent the large scale roughness from becoming too large. The impact of this parameter on the model results will be discussed later.

The ITC-2015 used in the measurements described in Sec. II is a free flooded ring transducer which has a toriodal beam pattern. While the beam pattern for the particular transducer used in TREX13 was not measured at 3003 Hz, a different ITC-2015 was characterized prior to the 2006 Shallow Water experiment (Yang *et al.*, 2012). The beam pattern was axisymmetric about the z-axis, with a maximum value (0 dB) around the circumference of the transducer in the x-y plane and dropping at the z-axis to –9 dB at the top and –18 dB at the bottom. For the following data/model comparisons, we assume that the beam patterns of the two transducers are similar and use the measured beam pattern in Eq. (20).

The output of the model for both scattering cross-sections is compared to the measured PSD in Fig. 7. For this example, the integral in Eq. (19) was evaluated as a summation over y from –1000 to 1000 m with $\Delta y = 1$ m and used a maximum value of $m = 10$ for the number of reflections of each ray from the seafloor. Since the model treats the scattered field as incoherent, the model output is independent of the receiver position within the array. In order to reduce computation time, the model was evaluated at a single depth, $z = 10$ m. Note also that the model does not account for the direct propagation from the source to the receiver which produces the large peak in the PSD at 2999 Hz.

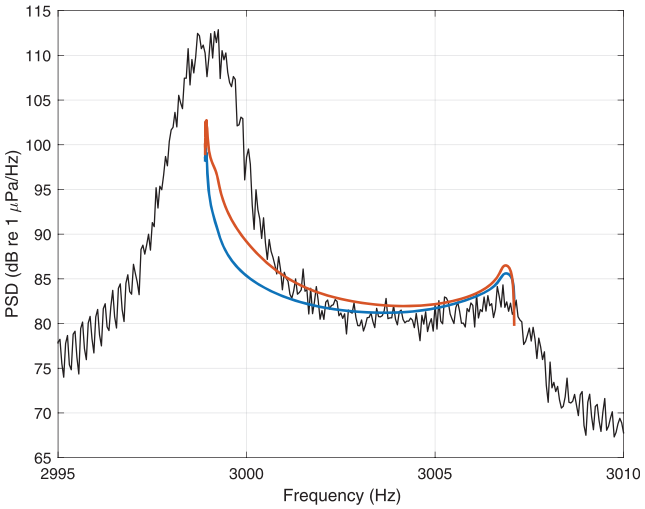

FIG. 7. (Color online) Comparison of the Doppler reverberation model given in Eq. (19) to the measured PSD in Fig. 4. The model used the parameters given in Table I with the scattering cross-section given by Lambert's law (dark blue line) and small-roughness perturbation theory (light red line).

The two scattering strength models give very similar results, both of which compare well to the measurement. The small-roughness perturbation theory result gives a slightly higher value than Lambert's law over most of the frequency range with the greatest difference occurring at those frequencies which correspond to the direct path peak. The scattering in this region is near specular and hence the perturbation result is a function of the low-wavenumber part of the roughness spectrum. This part of the spectrum is controlled by the choice of characteristic length. The reverberation level below f_0 can be increased by increasing the characteristic length and vice versa. While the choice of characteristic length used here was somewhat arbitrary, decreasing it beyond the value of 0.2 m will begin to affect the spectral fit in the measured band of wavenumbers (14.41–33.63 rad/m). Increasing it above this value will begin to significantly overestimate the spectral strength measured by Holland *et al.* at these low wavenumbers (Holland *et al.*, 2017). They used the measured bathymetry to estimate the spectral levels at the low wavenumbers and found the spectral levels are much lower than would be predicted if the characteristic length were allowed to become large.

At high frequencies, both model results predict a peak in the reverberation spectrum as the maximum Doppler frequency is approached. To understand the origin of this peak, consider the sound incident on the seafloor along the hyperbola corresponding to zero Doppler shift ($f = f_0$ or $\cos\theta_x = 0$). Along this hyperbola, the incident sound is above the critical angle, and hence suffering significant bottom loss until $\theta_{nm} = \theta_{crit}$, where θ_{crit} is the critical angle. As the amount of Doppler shift increases, the portion of the hyperbola for which the incident sound is above the critical angle decreases. When the Doppler shift reaches the point where $\theta_x = \theta_{crit}$, all the incident sound is below the critical angle and the bottom loss is greatly reduced. Just after this point, the reverberation peaks and then decreases as the scattering strength falls off as $\sin^2\theta$. This is seen clearly in Fig. 8 where the contributions of each of the multiply reflected rays are shown relative to the frequencies at which all rays become subcritical.

Figure 9 shows a comparison of the model output about $\Delta f = 0$ Hz to the spectral levels measured on both VLAs along each leg of the tow. Again both scattering strength expressions give similar results and compare well to the measurements when the source is greater than 500 m from the CPA. Near the CPA, the PSD at $\Delta f = 0$ Hz is dominated by the direct propagation which the model does not take into account. These range dependent model results use the local velocity of the ship which can vary along the legs causing slight differences in the reverberation levels. There are, however, no significant variations in either the model or the measurements and the range dependence is very similar with no dependence on the direction of the tow or distance from the VLA. This is consistent with the narrowband, monostatic

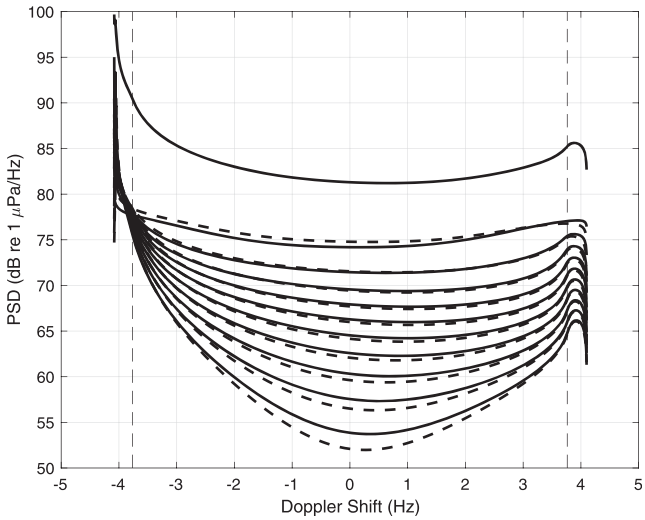

FIG. 8. The uppermost curve is the model result using Lambert's law for the scattering cross section (the blue curve in Fig. 7). Each curve below the model result is the contribution of the rays with m reflections and $n=0$ (black lines) and $n=1$ (dashed lines). Hence the first solid curve just below the model result is for $m=0$ and $n=0$, while the bottommost solid curve corresponds to $m=9$ and $n=0$. The vertical dashed lines correspond to those frequencies for which all of the incident sound is subcritical.

reverberation measurements made using a fixed source and horizontal line array at the TREX13 site. In those measurements, while it was possible to resolve range-dependent fluctuations in the broadband reverberation, the narrowband pulses ensonified larger portions of the seafloor and the reverberation level was a function of the mean scattering strength within those scattering patches. For the Doppler reverberation, the scattering patch size is determined by the frequency resolution, Δf, and the length and number of the ensonified hyperbolas [see Fig. 5(d)]. The smallest ensonified scattering patch therefore corresponds to $\Delta f=0$ Hz for which the scattering patch is essentially a strip of seafloor directly beneath the source and extending out perpendicular to the direction of travel. Even in this case, however, evaluation of the integral in Eq. (19) as a function of the limits of the integral finds that the length of the patch needs to be at least 1.6 km to provide an accurate result. As a result, this scattering patch averages out the fluctuations in the scattering strength detected in the narrowband reverberation yielding the smooth range dependence seen in Fig. 9.

V. DISCUSSION

While the TREX13 measurements discussed above were unable to detect any variation in the seafloor scattering, it may be possible to design a sonar that could exploit the Doppler reverberation for seabed characterization. Suppose that instead of an omnidirectional or toroidal source, one used a long thin source similar to side-scan and multibeam sources. Those sources are designed to have a very broad beam pattern in one direction with a narrow beam pattern in the perpendicular direction. In multibeam and side scan applications, the wide part of the beam is oriented such that it ensonifies a large swath of the seafloor underneath the tow body or vessel that is perpendicular to the direction of travel. If instead the source is rotated such that the wide portion of the beam is parallel to the direction of travel, only the center of the hyperbolas in Fig. 5(d) will be illuminated, greatly narrowing the portion of the seafloor from which the scattering is being measured. This is analogous to the Mill's cross configuration used in many multibeam sonars where the fan beams of a source and receiver are aligned perpendicular so that pencil beams can be formed. Here the frequency

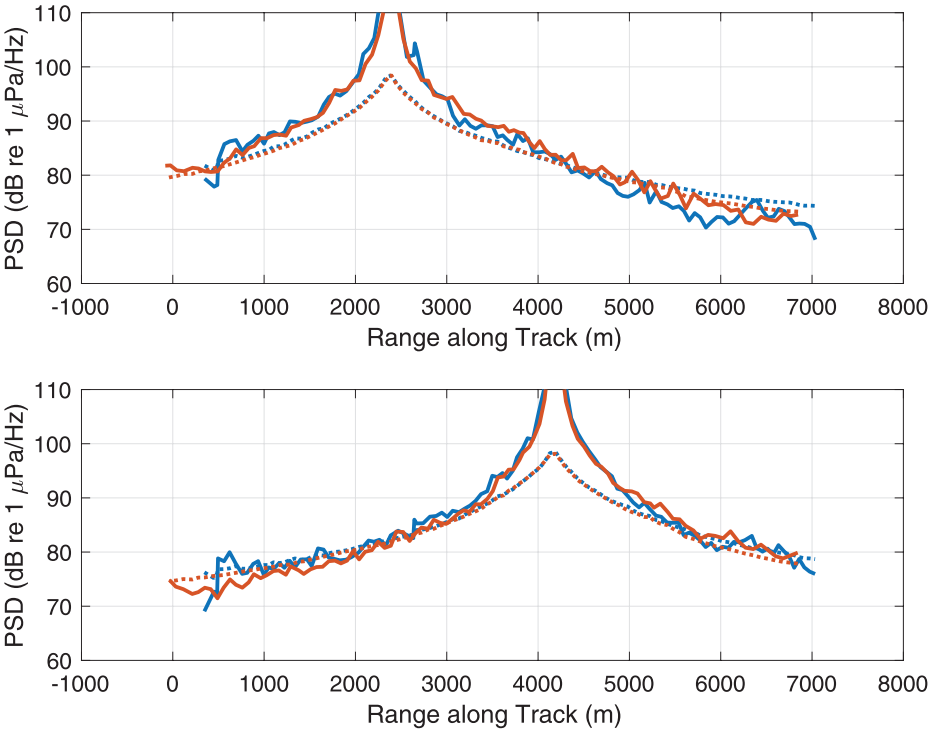

FIG. 9. (Color online) Comparison of the mean of the model result using Lambert scattering (dashed) to the mean of the measured PSD (solid) as a function of range along the track. The comparisons are both for Leg #1 (dark blue) and Leg #2 (light red) and received on VLA #1 (upper panel) and VLA #2 (lower panel). The mean was taken over the band of frequencies for which the Doppler shift varied from −1 to 1 Hz.

resolution provided by the Doppler reverberation replaces the beam pattern of the receiver.

In TREX13, the Doppler reverberation utilized a towed source and was measured on two, self-recording arrays of receivers deployed along the track. Compared to the co-located source and receiver required to measure direct-path scattering or monostatic, long-range reverberation, the sonar system considered above requires more equipment and presents additional logistical challenges to make a similar measurement. However, a direct path scattering measurement is often limited by the timing of multipath arrivals and only a portion of the bistatic scattering cross section can be measured (Holland *et al.*, 2000). A monostatic reverberation measurement avoids this issue by measuring the reverberation over a longer time and incorporating the multipath into the model fit. The difficulty with this measurement is that the model fit requires that the transmission loss is also modeled well since uncertainties in the transmission loss can produce uncertainties in the scattering cross-section estimate. This method also only samples the subcritical grazing angles in the scattering cross section since the sound propagating at higher angles is lost more rapidly to the seafloor.

The model fit to the Doppler reverberation measurement also requires modeling the transmission loss, however the bistatic source and receiver configuration provides the opportunity to make a simultaneous, independent measurement of the transmission loss. The towed source additionally makes this loss measurement a function of range. The Doppler reverberation measurement also provides a broader range of angles for the scattering strength, sampling angles both above and below the critical angle. It may also be possible to co-locate the source and receiver on the same moving platform. This would introduce an additional Doppler shift due to the moving receiver and also eliminate the transmission loss measurement, but it would reduce the equipment needed and allow for wide-area assessments of the seafloor scattering.

The model developed here considered only the Doppler spectrum but to fully consider this reverberation in the context of sonar performance prediction, the time component needs to be considered as well. This will require a combination of both scattering diagrams shown in Figs. 5(b) and 5(d) and the model developed in Sec. III can serve as a starting point for a time-frequency model. This would also make it possible to explore broadband transmissions from moving platforms and how the Doppler reverberation impacts sonar performance for different waveforms. The current model should also be expanded to consider additional environmental effects such as arbitrary sound speed profiles, sea surface roughness, and bathymetric variations.

VI. SUMMARY

A model for the frequency dependence of a narrowband signal transmitted from a moving source has been developed using a combination of rays, normal modes, and ray-mode analogies. Using environmental parameters consistent with values from environmental measurements conducted during TREX13, the model results were compared to towed source data also collected during that experiment. The model results compared favorably with the data both in frequency and range along the measurement track. The model used both Lambert's law and small roughness perturbation theory and although both provided similar results, perturbation theory used direct measurements of the seafloor properties while Lambert's law used an input parameter determined from a fit to previously analyzed data. The Doppler reverberation could potentially form the basis of a seafloor characterization technique if a source with limited directionality were used. The Doppler reverberation due to seafloor scattering may have an impact on sonar performance prediction particularly with regards to the use of Doppler to discriminate targets from reverberation and clutter.

ACKNOWLEDGMENTS

This research was supported by the U.S. Office of Naval Research under Grant Nos. N00014-16-1-2999 and N00014-12-1-0513.

Brown, M. V., and Frisk, G. V. (**1974**). "Frequency smearing of sound forward-scattered from the ocean surface," J. Acoust. Soc. Am. **55**(4), 744–749.

Bucker, H. P., and Morris, H. E. (**1968**). "Normal-mode reverberation in channels or ducts," J. Acoust. Soc. Am. **44**(3), 827–828.

Dall'Osto, D. R., Choi, J. W., and Dahl, P. H. (**2016**). "Measurement of acoustic particle motion in shallow water and its application to geoacoustic inversion," J. Acoust. Soc. Am. **139**(1), 311–319.

De Moustier, C. (**2014**). "Persistence of sharp acoustic backscatter transitions observed in repeat 400 kHz multibeam echosounder surveys offshore Panama City, Florida, over 1 and 24 months," J. Acoust. Soc. Am. **136**, 2267.

Ellis, D. (**1995**). "A shallow-water normal-mode reverberation model," J. Acoust. Soc. Am. **97**(5), 2804–2814.

Ellis, D. D. (**1993**). "Shallow water reverberation: Normal-mode model predictions compared with bistatic towed-array measurements," IEEE J. Ocean. Eng. **18**(4), 474–482.

Ellis, D. D., and Crowe, D. V. (**1991**). "Bistatic reverberation calculations using a three-dimensional scattering function," J. Acoust. Soc. Am. **89**(5), 2207–2214.

Ellis, D. D., Yang, J., Preston, J. R., and Pecknold, S. (**2017**). "A normal mode reverberation and target echo model to interpret towed array data in the target and reverberation experiments," IEEE J. Ocean. Eng. **42**(2), 344–361.

Hefner, B. T. (**2017**). "Characterization of seafloor roughness to support modeling of midfrequency reverberation," IEEE J. Ocean. Eng. **42**(4), 1110–1124.

Holland, C., Hollett, R., and Troiano, L. (**2000**). "Measurement technique for bottom scattering in shallow water," J. Acoust. Soc. Am. **108**(3), 997–1011.

Holland, C. W., Pinson, S., Smith, C. M., Hines, P. C., Olson, D. R., Dosso, S. E., and Dettmer, J. (**2017**). "Seabed structure inferences from TREX13 reflection measurements," IEEE J. Ocean. Eng. **42**(2), 268–288.

Hurdle, B. G., Ferris, R. H., and Flowers, K. D. (**1964**). "Effect of transducer velocity on the structure of signals scattered from the ocean bottom," J. Acoust. Soc. Am. **36**(10), 1936–1942.

Jackson, D. R., and Richardson, M. (**2006**). *High-Frequency Seafloor Acoustics* (Springer, New York).

Jensen, F. B., Kuperman, W. A., Porter, M. B., and Schmidt, H. (**2011**). *Computational Ocean Acoustics*, 2nd ed. (Springer, New York), pp. 143–147.

Lynch, S. D., and D'Spain, G. L. (**2012**). "Evidence of Doppler-shifted Bragg scattering in the vertical plane by ocean surface waves," J. Acoust. Soc. Am. **131**(3), 2011–2022.

McCammon, D. F., and McDaniel, S. T. (**1990**). "Spectral spreading from surface bubble motion," IEEE J. Ocean. Eng. **15**(2), 95–100.

Skolnik, M. I. (**2001**). *Introduction to Radar Systems*, 3rd ed. (McGraw-Hill, New York), pp. 171–182.

Thorsos, E. I., Tang, D., Williams, K. L., Hefner, B. T., and Yang, J. (**2011**). "Key issues in mid frequency reverberation modeling and experiments,"

in *Proceedings of the Conference on Underwater Acoustic Measurements*, Kos, Greece.

Wild, M., and Joyce, R. (**1995**). "Modeling the spatial and frequency distribution of narrow-band acoustic signals scattering from the ocean surface," J. Acoust. Soc. Am. **97**(3), 1559–1565.

Yang, J., Jackson, D. R., and Tang, D. (**2012**). "Mid-frequency geoacoustic inversion using bottom loss data from the shallow water 2006 experiment," J. Acoust. Soc. Am. **131**(2), 1711.

Yang, J., and Tang, D. (**2017**). "Direct measurements of sediment sound speed and attenuation in the frequency band of 2 – 8 kHz at the target and reverberation experiment site," IEEE J. Ocean. Eng. **42**(4), 1102–1109.

Yang, J., Tang, D., Hefner, B. T., Williams, K. L., and Preston, J. R. (**2018**). "Overview of midfrequency reverberation data acquired during the target and reverberation experiment 2013," IEEE J. Ocean. Eng. **43**(3), 563–585.

REPORT DOCUMENTATION PAGE

Form Approved
OMB No. 0704-0188

1. REPORT DATE *(DD-MM-YYYY)*	2. REPORT TYPE	3. DATES COVERED *(From - To)*
10-04-2020	Final	08/01/2016-07/31/2019

4. TITLE AND SUBTITLE

TREX13 Transmission Loss and Sea Floor Scattering Analysis Modeling

5a. CONTRACT NUMBER

5b. GRANT NUMBER

N00014-16-1-2999

5c. PROGRAM ELEMENT NUMBER

6. AUTHOR(S)
Brian T Hefner
Applied Physics Laboratory
University of Washington

5d. PROJECT NUMBER

5e. TASK NUMBER

5f. WORK UNIT NUMBER

7. PERFORMING ORGANIZATION NAME(S) AND ADDRESS(ES)

Applied Physics Laboratory
University of Washington
1013 NE 45th Street
Seattle, WA 98105-6698

8. PERFORMING ORGANIZATION REPORT NUMBER

9. SPONSORING/MONITORING AGENCY NAME(S) AND ADDRESS(ES)

Office of Naval Research
Dr. Raymond Soukup
875 N. Randolph Street
Arlington, VA 22203-1995

10. SPONSOR/MONITOR'S ACRONYM(S)

ONR

11. SPONSOR/MONITOR'S REPORT NUMBER(S)

12. DISTRIBUTION/AVAILABILITY STATEMENT

Distribution A: Approved for public release; distribution is unlimited

13. SUPPLEMENTARY NOTES

14. ABSTRACT

This work focuses on databasing and analyzing mid-frequency acoustic data collected on vertical line arrays (VLAs) during the Target and Reverberation Experiment in 2013 (TREX13). Data was collected for both a seafloor-mounted source and a ship-towed source. The signals received from the fixed source were incorporated into a common database with the reverberation data measured for the same transmissions. This database was used to analyze the transmission loss (TL) as a function of time to understand the impacts of changing environmental conditions on mid-frequency propagation and reverberation. The data from the towed-source was used to model reverberation associated with the Doppler-shifted signals. The transmission loss as a function of range was also used to develop a geoacoustic model of the seafloor that accounts for the spatial variability of the seafloor properties.

15. SUBJECT TERMS

TREX13, mid-frequency sonar, transmission loss, reverberation, Doppler, sediment acoustics

16. SECURITY CLASSIFICATION OF:			17. LIMITATION OF ABSTRACT	18. NUMBER OF PAGES	19a. NAME OF RESPONSIBLE PERSON
a. REPORT	b. ABSTRACT	c. THIS PAGE			Brian T Hefner
U	U	U	SAR	20	19b. TELEPHONE NUMBER *(Include area code)* 206-616-7558